ACS Infectious Diseases

pubs.acs.org/journal/aidcbc

Article

Drug-Repurposing Screening Identified Tropifexor as a SARS-CoV-2 Papain-like Protease Inhibitor

Chunlong Ma,[§] Yanmei Hu,[§] Yuyin Wang, Juliana Choza, and Jun Wang*

Cite This: https://doi.org/10.1021/acsinfecdis.1c00629

Read Online

ACCESS | Metrics & More | Article Recommendations

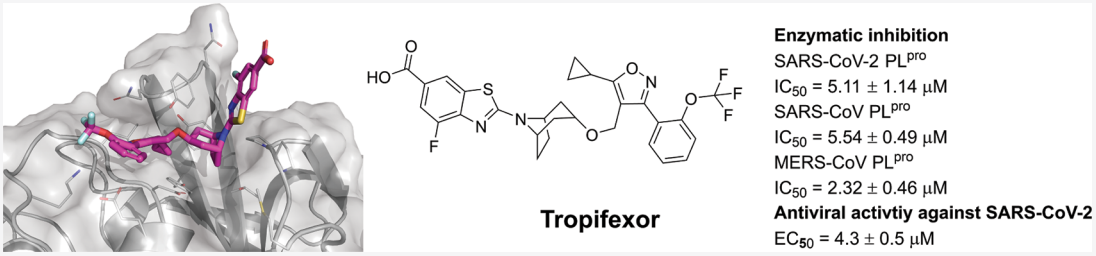

ABSTRACT: The global COVID-19 pandemic underscores the dire need for effective antivirals. Encouraging progress has been made in developing small-molecule inhibitors targeting the SARS-CoV-2 RNA-dependent RNA polymerase (RdRp) and main protease (M^{pro}). However, the development of papain-like protease (PL^{pro}) inhibitors faces several obstacles. Nevertheless, PL^{pro} represents a high-profile drug target given its multifaceted roles in viral replication. PL^{pro} is involved in not only the cleavage of viral polyprotein but also the modulation of host immune response. In this study, we conducted a drug-repurposing screening of PL^{pro} against the MedChemExpress bioactive compound library and identified three hits, EACC, KY-226, and tropifexor, as potent PL^{pro} inhibitors with IC_{50} values ranging from 3.39 to 8.28 μM. The three hits showed dose-dependent binding to PL^{pro} in the thermal shift assay. In addition, tropifexor inhibited the cellular PL^{pro} activity in the FlipGFP assay with an IC_{50} of 10.6 μM. Gratifyingly, tropifexor showed antiviral activity against SARS-CoV-2 in Calu-3 cells at noncytotoxic concentrations. Overall, tropifexor represents a novel PL^{pro} inhibitor that can be further developed as SARS-CoV-2 antivirals.

KEYWORDS: *SARS-CoV-2, papain-like protease, PL^{pro}, antiviral, tropifexor, GRL0617*

The etiological agent of COVID-19 is SARS-CoV-2, a single-stranded, positive-sense RNA virus that belongs to the β-coronavirus genera. Given the catastrophic impact of COVID-19 on public health and global economy, researchers around the globe are working relentlessly to develop vaccines and antiviral drugs. This effort led to the approval of vaccines and antiviral drugs at a record-breaking speed. Two mRNA vaccines from Moderna and Pfizer and one adenovirus-based vaccine from Johnson & Johnson were approved by FDA.[1]

Although vaccines are the mainstay in combating the pandemic, antiviral drugs are nevertheless needed as complementary strategies. Vaccines are preventative, while antiviral drugs can be used for the treatment of COVID patients. In addition, the mRNA vaccines target the viral spike protein, which is prone to mutation as shown by the variants of concerns including the Delta variant and the most recent Omicron variant.[2] As a result, vaccines might need to be frequently updated to match the circulating strains. In comparison, small-molecule antiviral drugs targeting the conserved viral proteins are expected to have broad-spectrum antiviral activity and a high genetic barrier to drug resistance. The viral RNA-dependent RNA polymerase (RdRp) inhibitor remdesivir is the first FDA-approved COVID drug.[3] In addition, the second RdRp inhibitor molnupiravir[4−6] and the main protease (M^{pro}) inhibitor PF-07321332 (Nirmatrelvir in Paxlovid)[7] are FDA-approved specific oral COVID drugs.

Despite the encouraging progress, additional antiviral drugs with a novel mechanism of action are still in dire need to override the emergence of new mutations. They can be used either alone or in combination with existing RdRp inhibitors or M^{pro} inhibitors to combat not only the current COVID-19 pandemic but also future coronavirus outbreaks.

SARS-CoV-2 expresses two viral proteases, the M^{pro} and papain-like protease (PL^{pro}), during viral replication. Both M^{pro} and PL^{pro} are cysteine proteases that mediate the cleavage of viral polyprotein during viral replication.[8] In addition, PL^{pro} dysregulates the host immune responses by cleaving ubiquitin and interferon-stimulated gene 15 protein (ISG15) from host

Received: December 1, 2021

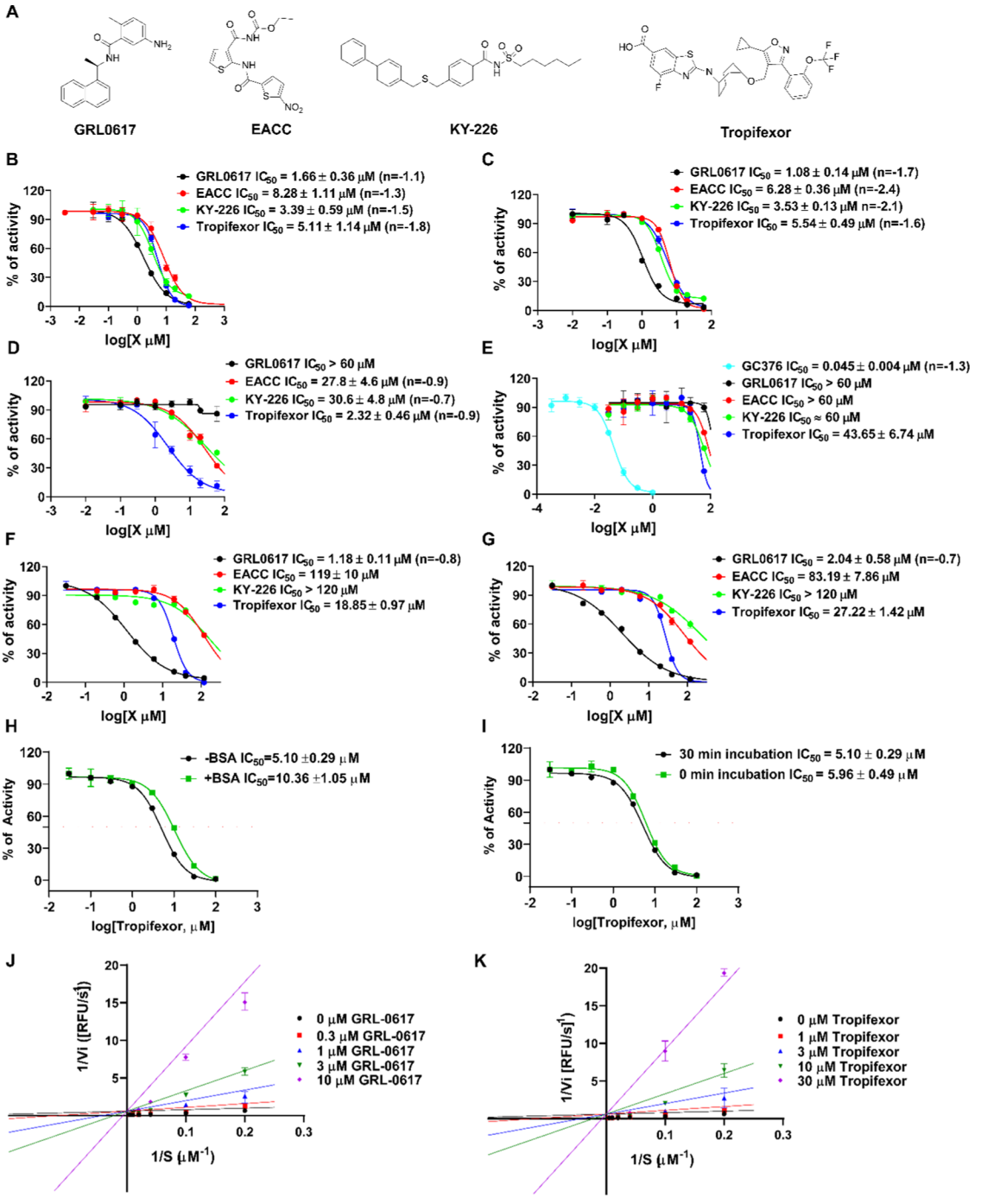

Figure 1. Characterization of SARS-CoV-2 PL^{pro} inhibitors identified from the high-throughput screening. (A) Chemical structures of the positive control GRL0617 and the three hits EACC, KY-226, and tropifexor. (B) IC_{50} curves of the hits in inhibiting SARS-CoV-2 PL^{pro} with the FRET peptide substrate 1. (C) IC_{50} curves of the hits in inhibiting SARS-CoV PL^{pro} with the FRET peptide substrate 1. (D) IC_{50} curves of the hits in inhibiting MERS-CoV PL^{pro} with the FRET peptide substrate 1. (E) IC_{50} curves of the hits in inhibiting SARS-CoV-2 M^{pro} with the FRET peptide substrate 2. (F) IC_{50} curves of the hits in inhibiting SARS-CoV-2 PL^{pro} with the Ub-AMC substrate. (G) IC_{50} curves of the hits in inhibiting SARS-CoV-2 PL^{pro} with the ISG15-AMC substrate. Please refer to the Materials and Methods section for assay conditions. Values represent the average ± standard deviation of three replicates. (H) IC_{50} curves of tropifexor in inhibiting SARS-CoV-2 PL^{pro} with and without the addition of 0.01% BSA. (I) IC_{50} curves of tropifexor in inhibiting SARS-CoV-2 PL^{pro} with or without a 30 min preincubation. (J) Lineweaver−Burk curves of GRL0617 in inhibiting SARS-CoV-2 PL^{pro}. (K) Lineweaver−Burk curves of tropifexor in inhibiting SARS-CoV-2 PL^{pro}.

proteins.[9] Therefore, inhibiting PL^{pro} is a two-pronged approach to protecting host cells from viral infection.

PL^{pro} is a 35 kDa domain withinNsp3, which is a 215 kDa multidomain protein that is a key component of the viral replication complex.[10] Compared to PL^{pro} from SARS-CoV, SARS-CoV-2 PL^{pro} displays decreased deubiquitination activity and enhanced deISGlyation activity.[9,11]

In contrast to M^{pro}, PL^{pro} is a more challenging drug target mainly for two reasons. First, the protein substrate of PL^{pro} consists of LXGG.[12] Accordingly, there is a lack of drug

https://doi.org/10.1021/acsinfecdis.1c00629
ACS Infect. Dis. XXXX, XXX, XXX−XXX

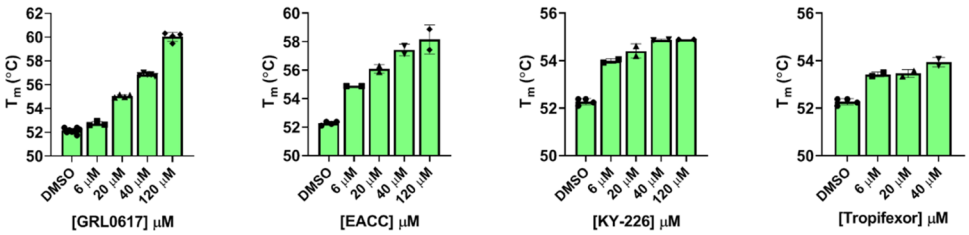

Figure 2. Thermal shift assay of SARS-CoV-2 PL^{pro} protease against identified inhibitors. All inhibitors display a dose-dependent melting temperature (T_m) shift. Values represent the average ± standard deviation of three replicates.

binding pockets in the S1 and S2 subsites. As such, a majority of reported PL^{pro} inhibitors are noncovalent inhibitors that bind to the S3 and S4 subsites that are located more than 10 Å away from the catalytic cysteine C111.[13−15] Second, PL^{pro} cleaves the same substrate sequence LXGG as the human deubiquitinase,[16] which presents a challenge in developing selective PL^{pro} inhibitors. Despite extensive high-throughput screening and lead optimization,[11,13−15,17,18] GRL0617 and its analogues remain the most potent PL^{pro} inhibitors reported so far. To identify structurally novel PL^{pro} inhibitors, we conducted a drug-repurposing screening and identified EACC, KY-226, and tropifexor as potent PL^{pro} inhibitors with IC_{50} values ranging from 3.39 to 8.28 μM. EACC is a reversible autophagy inhibitor.[19] KY-226 is a potent, selectivity, and orally bioavailable allosteric protein tyrosine phosphatase 1B (PTP1B) with an IC_{50} of 0.25 μM.[20] Tropifexor is a highly potent agonist of the farnesoid X receptor and is currently undergoing phase II clinical trial for nonalcoholic steatohepatitis (NASH) and liver fibrosis.[21] Their antiviral mechanism of action was further characterized in the thermal shift assay and the FlipGFP protease assay. Gratifyingly, tropifexor also had potent antiviral activity against SARS-CoV-2 in Calu-3 cells with an EC_{50} of 4.03 μM. Overall, tropifexor represents a potent PL^{pro} inhibitor with a novel scaffold that can be further developed as SARS-CoV-2 antivirals.

RESULTS AND DISCUSSION

High-Throughput Screening of SARS-CoV-2 PL^{pro} Inhibitors. Using the previously optimized FRET assay condition,[15] we performed a high-throughput screening of SARS-CoV-2 PL^{pro} against the MedChemExpress bioactive compound library, which consists of 9,791 compounds including FDA-approved drugs, clinical candidates, and natural products. The assay was performed in a 384-well plate with a Z' of 0.688, and GRL0617 was included as the positive control. All compounds were originally screened at 40 μM, and hits showing more than 50% inhibition were further titrated to determine the IC_{50} values. GRL0617 was included as a positive control. In total, three compounds, EACC, KY-226, and tropifexor (Figure 1A), were identified as positive hits with IC_{50} values of 8.28, 3.39, and 5.11 μM, respectively (Figure 1B). In comparison, the IC_{50} value for the positive control GRL0617 was 1.66 μM (Figure 1B). Next, the broad-spectrum activity of the three hits was tested against SARS-CoV PL^{pro} (Figure 1C) and MERS-CoV PL^{pro} (Figure 1D). It was found that EACC, KY-226, and tropifexor retained potent inhibition against SARS-CoV PL^{pro} with IC_{50} values of 6.28, 3.53, and 5.54 μM, respectively (Figure 1C). In contrast, EACC and KY-226 were weak inhibitors of MERS-CoV PL^{pro} with IC_{50} values of 27.8 and 30.6 μM, while GRL0617 was inactive (IC_{50} > 60 μM) (Figure 1D). Nevertheless, tropifexor showed higher potency against MERS-CoV PL^{pro} with an IC_{50} of 2.32 μM (Figure 1D). The hits were further counterscreened against the SARS-CoV-2 M^{pro} to rule out promiscuous cysteine protease inhibitors.[22−25] It was found that EACC and KY-226 were not active ($IC_{50} \geq 60$ μM), while tropifexor had weak inhibition with an IC_{50} of 43.65 μM, which corresponds to a selectivity index (SI) of 8.5 (Figure 1E). These results suggest that the inhibition of SARS-CoV-2 PL^{pro} by tropifexor is specific. The inhibition of PL^{pro}'s deubiquitination and deISGlyation activities was characterized using the Ub-AMC and ISG15-AMC substrates, respectively.[14,15] While EACC and KY-226 were inactive in inhibiting the deubiquitinase activity of PL^{pro} (IC_{50} > 100 μM), tropifexor showed moderate activity with an IC_{50} of 18.85 μM (Figure 1F). Similarly, EACC and KY-226 were not active in inhibiting the deISGlyation activity of PL^{pro} (IC_{50} > 80 μM), tropifexor showed does-dependent inhibition with an IC_{50} of 27.22 μM (Figure 1G). Tropifexor is a hydrophobic compound with a $C\log P$ of 5.69. To rule out the possibility that the observed PL^{pro} inhibition was due to nonspecific binding, we repeated the FRET assay against SARS-CoV-2 PL^{pro} in the presence of 0.01% BSA, and it was found that tropifexor retained potent inhibition with an IC_{50} of 10.36 μM (Figure 1H), suggesting that the inhibition of PL^{pro} by tropifexor is unlikely due to nonspecific hydrophobic interactions. Tropifexor had similar IC_{50} values against SARS-CoV-2 PL^{pro} with and without a 30 min preincubation (Figure 1I), suggesting a reversible binding. The mechanism of inhibition of tropifexor was further studied in an enzymatic kinetic experiment, and GRL0617 was included as a control. The Lineweaver−Burk plots showed that both GRL0617 and tropifexor are competitive inhibitors of SARS-CoV-2 PL^{pro} (Figure 1J,K).

Overall, tropifexor appears to be the most promising hit with consistent inhibition against SARS-CoV-2, SARS-CoV, and MERS-CoV PL^{pro}s. In addition, tropifexor also inhibited the deubiquitination and deISGlyation activities of SARS-CoV-2 PL^{pro}, albeit at lower potency.

Pharmacological Characterization of the Hits in the Thermal Shift Assay and the Cell-Based FlipGFP PL^{pro} Assay. The mechanism of action of EACC, KY-226, and tropifexor in inhibiting SARS-CoV-2 PL^{pro} was further characterized by the thermal shift assay and the cell-based FlipGFP PL^{pro} assay.[15,22,23,26] Thermal shift assay measures the direct binding between the compound and the protein; therefore, it can rule out hits that might bind to the FRET substrate in the enzymatic assay. Similar to the positive control GRL0617, all three hits displayed dose-dependent binding to PL^{pro}, as revealed by the enhanced melting temperatures with increasing drug concentrations (Figure 2).

Next, we tested the three hits in the FlipGFP PL^{pro} assay.[15,22,23] The FlipGFP PL^{pro} was recently developed by

https://doi.org/10.1021/acsinfecdis.1c00629
ACS Infect. Dis. XXXX, XXX, XXX−XXX

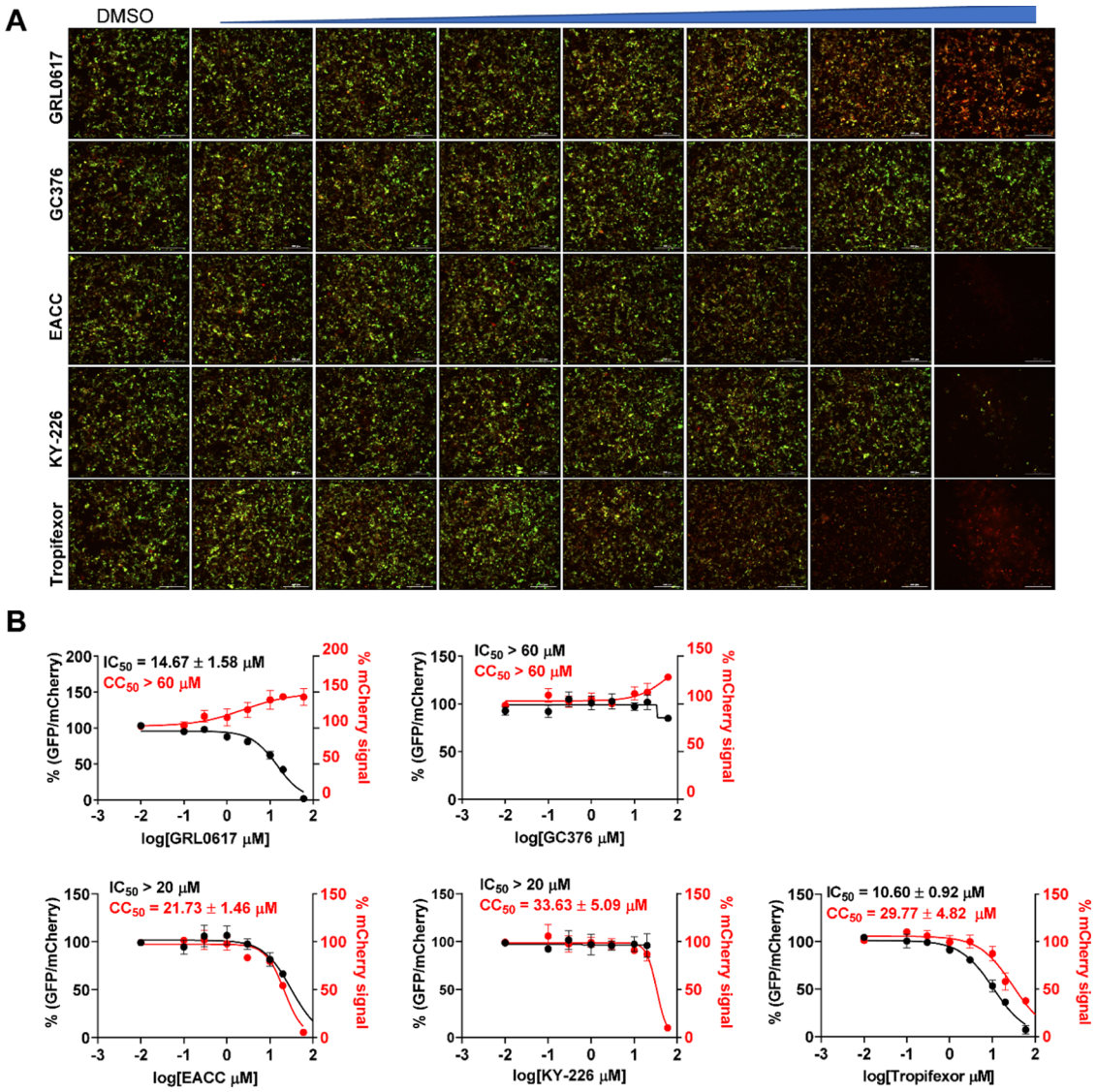

Figure 3. FlipGFP SARS-CoV-2 PL^{pro} assay to determine the cellular protease inhibitory activity of identified inhibitors. (A) Representative images of FlipGFP PL^{pro} assay with increasing concentrations of GRL0617 (positive control), GC376 (negative control), EACC, KY-226, and tropifexor. GRL0617 showed a dose-dependent decrease of GFP signal with the increasing drug concentration, while almost no GFP signal change was observed with the increasing concentration of negative control compound GC376. (B) Dose−response curves of the GFP/mCherry ratio with increasing drug concentrations. mCherry signal alone was used to calculate the transfection efficiency and compound cytotoxicity. All three hits displayed significant cytotoxicity at high drug concentrations. Values represent the average ± standard deviation of three replicates.

us as a surrogate assay to quantify the cellular activity of PL^{pro} inhibitors in the biological safety level 2 facility, and we have shown that there is a positive correlation between the FlipGFP IC_{50} values with the SARS-CoV-2 antiviral EC_{50} values.[15] The FlipGFP assay is a virus-free cell-based protease assay in which the 293T cells were transfected with PL^{pro} and the GFP reporter. The GFP reporter consists of two fragments,[27,28] the β1−9 template and the β10-11 strands that are constrained in the parallel inactive conformation through a PL^{pro} substrate linker. Upon cleavage of the substrate linker, the β10 and β11 strands become parallel and can associate with the β1−9 template, leading to increased GFP signal. mCherry is included as an internal control to normalize transfection efficacy and compound cytotoxicity. In principle, the normalized GFP/mCherry ratio is proportional to the enzymatic activity of PL^{pro}. The advantage of the FlipGFP assay over the FRET assay is that it can rule out compounds that are cytotoxic, membrane-impermeable, and having off-target effects that prevent cellular on-target engagement.[22,23]

In the FlipGFP assay, the positive control GRL0617 showed dose-dependent inhibition with an IC_{50} of 14.67 μM, while the negative control GC376 was not active (IC_{50} > 60 μM) (Figure 3A,B). The results from EACC and KY-226 were not conclusive due to the cell cytotoxicity of the compounds. Tropifexor had an IC_{50} of 10.60 μM but a low selectivity index (CC_{50} = 29.77 μM, SI = 2.8) (Figure 3A,B). Given the low selectivity, the results from the FlipGFP are not stringently conclusive. Nevertheless, tropifexor reduced the GFP/mCherry ratio by 50% at 10 μM, which was not cytotoxic. In summary, the FlipGFP assay results suggest that tropifexor might have antiviral activity against SARS-CoV-2.

Antiviral Activity of Hits against SARS-CoV-2 in Calu-3 Cells. The antiviral activity of EACC, KY-226, and tropifexor in inhibiting SARS-CoV-2 replication in Calu-3 cells was tested

https://doi.org/10.1021/acsinfecdis.1c00629
ACS Infect. Dis. XXXX, XXX, XXX−XXX

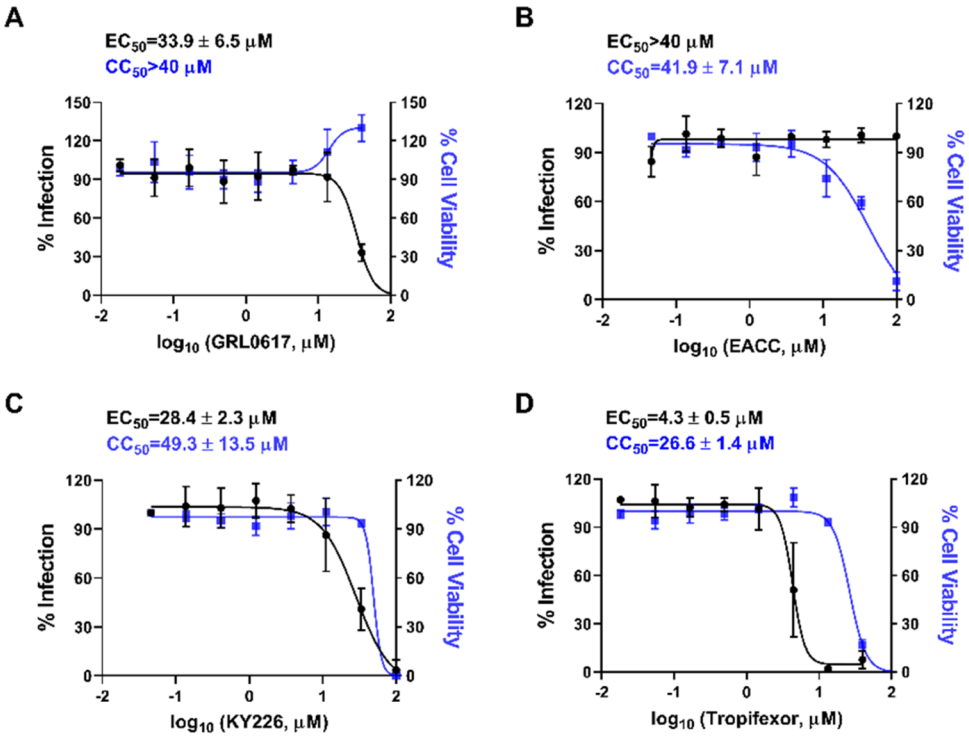

Figure 4. Antiviral activity of SARS-CoV-2 PL^{pro} inhibitors GRL0617 (A), EACC (B), KY-226 (C), and tropifexor (D) against SARS-CoV-2 in Calu-3 cells. The results were quantified by immunofluorescence assay. Values represent the average ± standard deviation of three replicates.

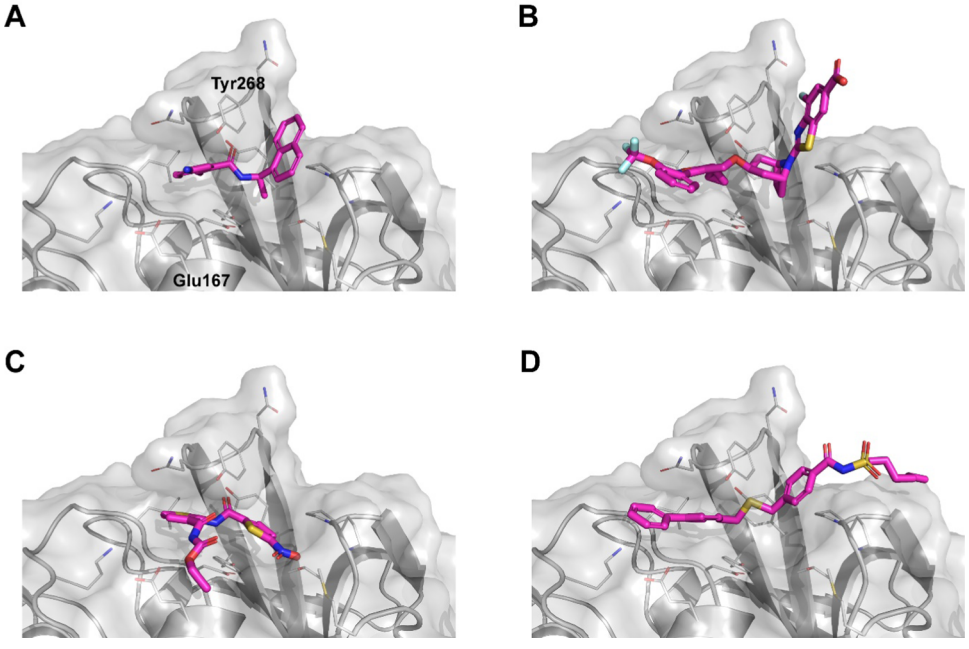

Figure 5. Molecular docking of SARS-CoV-2 PL^{pro} inhibitors GRL0617 (A), tropifexor (B), EACC (C), and KY-226 (D) in PL^{pro} (PDB: 7JRN). The Glide scores are −7.161 (GRL0617), −4.085 (tropifexor), −3.794 (EACC), and −3.332 (KY-226).

using the immunofluorescence assay (Figure 4). Calu-3 is TMPRSS2-positive and is a close mimetic of the human respiratory epithelial cells,[29] enabling it a widely accepted cell line for SARS-CoV-2 studies.[22,30] The positive control GRL0617 had an EC_{50} of 31.4 μM (Figure 4A). EACC did not show antiviral activity at nontoxic drug concentration (EC_{50} > 35 μM, CC_{50} = 35.29 μM) (Figure 4B). Gratifyingly, both KY-226 and tropifexor had improved antiviral activity against SARS-CoV-2 with EC_{50} values of 25.0 (Figure 4C) and 4.03 μM (Figure 4D), respectively. While KY-226 had a low selectivity index (SI = 1.65), tropifexor had a moderate selectivity window (SI = 6.97) and the observed antiviral activity was likely not caused by the cytotoxicity of the compound.

Molecular Docking of EACC, KY-226, and Tropifexor in SARS-CoV-2 PL^{pro}. To gain insights into the binding mode of the three hits, we performed molecular docking with Schrödinger Glide XP (extra precision) using the wild-type

https://doi.org/10.1021/acsinfecdis.1c00629
ACS Infect. Dis. XXXX, XXX, XXX−XXX

SARS-CoV-2 PL^{pro} structure we recently solved (PDB: 7JRN).[15] The binding sites were calculated by site map, and the GRL0617 binding site was identified as the top-ranked binding site; therefore, it was selected for docking. GRL0617 was included as a positive control. The docking pose of GRL0617 was superimposable with the binding mode in the X-ray crystal structure (Figure 5A). Tropifexor, EACC, and KY-226 all fit snuggly into the U-shaped binding pocket that is covered by the BL2 loop where GRL0617 binds (Figure 5B–D). Among the three hits, tropifexor showed the most favorable binding pose with a Glide score of −4.085 (Figure 5B). The docking poses might provide a guidance for the following lead optimization.

CONCLUSIONS

Although PL^{pro} is a validated antiviral drug target, the development of PL^{pro} inhibitors falls behind M^{pro} and RdRp inhibitors. As of date, no PL^{pro} inhibitors have been advanced to the *in vivo* animal model studies yet. The naphthalene compounds such as GRL0617 and its analogues are the only class of validated PL^{pro} inhibitors with antiviral activity against SARS-CoV-2. However, the low metabolic stability of this series of compounds might prevent its further development.[14,31] In this study, we aimed to identify structurally novel PL^{pro} inhibitors that can serve as starting points for further optimization. Through screening the MedChemExpress bioactive compound library, three hits EACC, KY-226, and tropifexor were identified as SARS-CoV-2 PL^{pro} inhibitors with IC_{50} values in the single-digit micromolar range. Among the three hits, tropifexor appears to be the most promising hit as it also showed potent inhibition against SARS-CoV PL^{pro} (IC_{50} = 5.54 μM) and MERS-CoV PL^{pro} (IC_{50} = 2.32 μM). In addition to the inhibition of the PL^{pro}-mediated cleavage of the viral polyprotein substrate, tropifexor also inhibited the deubiquitination and deISGlyation activities of SARS-CoV-2 PL^{pro}. Consistent with the enzymatic inhibition, tropifexor showed a dose-dependent stabilization of SARS-CoV-2 PL^{pro} in the thermal shift assay. Importantly, tropifexor displayed cellular PL^{pro} inhibitory activity in the FlipGFP assay and the antiviral activity against SARS-CoV-2 in Calu-3 cells. Although the low selectivity index (SI = 6.2) of tropifexor in the antiviral assay prevents its direct repurposing as a SARS-CoV-2 antiviral, the discovery of tropifexor as a novel PL^{pro} inhibitor provides an additional scaffold for further medicinal chemistry optimization. Follow-up studies will focus on improving the target and cellular selectivity. Furthermore, tropifexor is a fairly large molecule (MW: 603.59); efforts will be made to reduce the size as well as the hydrophobicity of the compound to optimize ligand efficiency and druglikeness properties.

MATERIALS AND METHODS

Protein Expression and Purification. Detailed expression and purification procedures untagged SARS-CoV-2 PL^{pro} and SARS-CoV-2 M^{pro} were described in our previous publications.[15,32] SARS-CoV papain-like protease gene (ORF 1ab 1541-1855) (accession # AEA10621.1) from strain SARS coronavirus MA15 with *Escherichia coli* codon optimization in the pET28b-(+) vector was ordered from GenScript. Then, the SARS-CoV PL^{pro} gene (ORF 1ab 1541-1855) was subcloned from the pET28b-(+) to pE-SUMO vector according to the manufacturer's protocol (LifeSensors Inc., Malvern, PA). The forward primer with the Bsa I site is GCGGTCTCAAGGTGAGGTGAAGACCATCAAAGTGTTCACCACC; the reverse primer with a Bsa I site is GCGGTCTCTCTAGATTATTTAATGGTGGTGGTATAGCTGGTTTCCTTGTAG. The expression and purification protocol of SARS-CoV PL^{pro} are identical to those of SARS-CoV-2 PL^{pro}.[15]

MERS-CoV PL^{pro} gene (ORF 1ab 1482-1803) (accession # KY581684) from strain MERS coronavirus Hu/UAE_002_2013 with *E. coli* codon optimization in the pET28b-(+) vector was ordered from GenScript. Then, the MERS-CoV PL^{pro} gene (ORF 1ab 1482-1803) was subcloned into the pE-SUMO vector with the pair primers: GCGGTCTCAAGGTCAGCTGACCATC-GAGGTGCTGGTTACCGTGG and GCGGTCTCTCTA-GATTAGTTGCAATCGCTGCTATATTTTTGACCCGG-GAAC. The expression and purification protocol of MERS-CoV papain-like protease are identical to those of SARS-CoV-2 PL^{pro}.[15]

FRET Substrate Synthesis. The SARS-CoV-2 PL^{pro} FRET substrate 1 is Dabcyl-FTLRGG/APTKV(Edans); this substrate was also used as SARS-CoV PL^{pro} and MERS-CoV PL^{pro} substrates. SARS-CoV-2 M^{pro} FRET substrate 2 is Dabcyl-KTSAVLQ/SGFRKME- (Edans). These FRET substrates were synthesized by solid-phase synthesis through iterative cycles of coupling and deprotection using the previously optimized procedure.[33] Ub-AMC and ISG15-AMC were purchased from BostonBiochem (catalog nos. U-550-050 and UL-553-050, respectively).

Enzymatic Assays. The high-throughput screening was carried out in 384-well format, as described previously.[15] The bioactive compound library consisting of 9,791 compounds was purchased from MedChemExpress (catalog no. HY-L001). The enzymatic reactions for SARS-CoV-2, SARS-CoV, and MERS-CoV PL^{pro}s were carried out in a reaction buffer consisting of 50 mM HEPES pH 7.5, 5 mM DTT, and 0.01% Triton X-100. For the IC_{50} measurement with the FRET peptide−Edans substrate, the reaction was carried out in 96-well format with a 100 μL reaction volume. SARS-CoV-2 PL^{pro} (200 nM), SARS-CoV PL^{pro} (200 nM), or MERS-CoV PL^{pro} (2 μM) was preincubated with various concentrations of testing compounds at 30 °C for 30 min before the addition of the FRET peptide substrate to initiate the reaction. The reaction was monitored in a Cytation 5 image reader with filters for excitation at 360/40 nm and emission at 460/40 nm at 30 °C for 1 h. The initial enzymatic reaction velocity was calculated from the initial 10 min enzymatic reaction via a linear regression function and was plotted against the substrate concentrations in Prism 8 with a four-parameter dose−response function. For the IC_{50} measurements with Ub-AMC or ISG15-AMC substrate, the reaction was carried out in 384-well format in a 50 μL reaction volume. In the Ub-AMC cleavage assay, the final SARS-CoV-2 PL^{pro} concentration is 50 nM, and the substrate Ub-AMC concentration is 2.5 μM. In the ISG15-AMC assay, the final SARS-CoV-2 PL^{pro} concentration is 2 nM, and the substrate ISG15-AMC concentration is 0.5 μM. The SARS-CoV-2 M^{pro} enzymatic assays were carried out in the reaction buffer containing 20 mM HEPES pH 6.5, 120 mM NaCl, 0.4 mM EDTA, 20% glycerol, and 4 mM DTT, as described previously.[32,34]

To rule out that the inhibition of tropifexor on PL^{Pro} is due to aggregation, 200 nM PL^{Pro} was incubated with serial concentrations of tropifexor (0, 0.1, 0.3, 1, 3, 10, 30, 100 μM) in the reaction buffer in the presence or absence of 0.01% BSA (0.1 mg/mL) at 30 °C for 30 min. The reaction was initiated

https://doi.org/10.1021/acsinfecdis.1c00629
ACS Infect. Dis. XXXX, XXX, XXX−XXX

by adding a 10 μM FRET substrate and monitored every 90 s for 1 h at 30 °C. The initial velocity was determined in the first 15 min by linear regression. The IC_{50} values were determined by fitting the curves with nonlinear regression using log (concentration of inhibitor) vs response with variable slopes in Prism 8.

To determine whether preincubation affects the IC_{50} value of tropifexor, 200 nM PL^{Pro} was mixed with serial concentrations of tropifexor (0, 0.1, 0.3, 1, 3, 10, 30, 100 μM) in the reaction buffer with or without preincubation at 30 °C for 30 min, and the reaction was initiated by adding a 10 μM FRET substrate. IC_{50} values were determined as previously described.

To determine the binding mode of tropifexor, K_M and V_{max} were determined at different concentrations of GRL0617 (0, 0.3, 1, 3, 10 μM) or tropifexor (0, 1, 3, 10, 30 μM). SARS-CoV-2 PL^{Pro} (200 nM) was mixed with the indicated concentrations of GRL0617 or tropifexor in the reaction buffer and incubated at 30 °C for 30 min. The reaction was initiated by adding different concentrations of FRET peptides (5, 10, 25, 50, 100, 200 μM). Michaelis−Menten and Lineweaver−Burk curves were plotted in Prism 8.

Differential Scanning Fluorimetry (DSF). The thermal shift assay (TSA) was carried out using a Thermo Fisher QuantStudio 5 real-time PCR system, as described previously.[15,32] Briefly, 4 μM SARS-CoV-2 PL^{pro} protein in the PL^{pro} reaction buffer (50 mM HEPES pH 7.5, 5 mM DTT, and 0.01% Triton X-100) was incubated with various concentrations of testing compounds at 30 °C for 30 min. A 1× SYPRO orange dye was added, and the fluorescence of each well was monitored under a temperature gradient range from 20 to 90 °C with a 0.05 °C/s incremental step. The melting temperature (Tm) was calculated as the mid-log of the transition phase from the native to the denatured protein using a Boltzmann model in Protein Thermal Shift Software v1.3.

Cell-Based FlipGFP PL^{pro} Assay. Plasmid pcDNA3-PLpro-flipGFP-T2A-mCherry was constructed from pcDNA3-TEV-flipGFP-T2A-mCherry.[15] SARS-CoV-2 PL^{pro} expression plasmid pcDNA3.1-SARS2 PL^{pro} was ordered from Genscript (Piscataway NJ) with codon optimization. For transfection, 293T cells were seeded into a 96-well Greiner plate (catalog no. 655090) overnight with 70−90% confluency; 50 ng of pcDNA3-PLPro-flipGFP-T2A-mCherry plasmid and 50 ng of protease expression plasmid pcDNA3.1-PL^{pro} were added to each well in the presence of a transfection reagent TransIT-293 (Mirus) according to the manufacturer's protocol. Three hours after transfection, 1 μL of the testing compound was added to each well at 100-fold dilution. Images were acquired 2 days after transfection with a Cytation 5 imaging reader (Biotek) GFP and mCherry channels and were analyzed with Gen5 3.10 software (Biotek). SARS-CoV-2 PL^{pro} protease activity was calculated by the ratio of the GFP signal over the mCherry signal. The FlipGFP PL^{pro} assay IC_{50} value was determined by plotting the GFP/mCherry signal over the compound concentration with a four-parameter dose−response function in Prism 8. The mCherry signal alone was utilized to evaluate the transfection efficiency and compound cytotoxicity.

Antiviral Assay in Calu-3 Cells. Calu-3 cells (ATCC, HTB-55) grown in minimal Eagle's medium supplemented with 1% nonessential amino acids, 1% penicillin/streptomycin, and 10% FBS are plated in 384-well plates. The next day, 50 nL of drug suspended in DMSO is added as an 8-pt dose−response with 3-fold dilutions between test concentrations in triplicate, starting at 40 μM final concentration. The negative control (DMSO, n = 32) and positive control (10 μM remdesivir, n = 32) are included on each assay plate. Calu-3 cells are pretreated with controls and test drugs (in triplicate) for 2 h prior to infection. In BSL3 containment, SARS-CoV-2 (isolate USA-WA1/2020) diluted in a serum-free growth medium is added to plates to achieve an MOI = 0.5. Cells are incubated continuously with drugs and SARS-CoV-2 for 48 h. Cells are fixed and then immunostained with anti-dsRNA (J2), and nuclei are counterstained with Hoechst 33342 for automated microscopy. Automated image analysis quantifies the number of cells per well (toxicity) and the percentage of infected cells (dsRNA+ cells/cell number) per well. SARS-CoV-2 infection at each drug concentration was normalized to aggregated DMSO plate control wells and expressed as percentage of control (POC = % infection sample/Avg % infection DMSO cont). A nonlinear regression curve fit analysis (GraphPad Prism 8) of POC infection and cell viability versus the log 10 transformed concentration values to calculate EC_{50} values for infection and CC_{50} values for cell viability. Selectivity index (SI) was calculated as a ratio of drug's CC_{50} and EC_{50} values (SI = CC_{50}/IC_{50}).

Molecular modeling of the binding of EACC, KY-226, and tropifexor to SARS-CoV-2 PL^{pro}. Docking was performed using Schrödinger Glide extra precision (XP). The SARS-CoV-2 PL^{pro} structure was downloaded from the PDB code 7JRN. The binding sites were calculated by the site map, and the GRL0617 binding site is the highest-scored binding site, and therefore, it was chosen for docking. The docking grid was centered around GRL0617 with the coordinates of X = 9.88, Y = −11.74, and Z = 32.55. GRL0617 was added as a positive control for the docking. The final docking poses were generated in PyMOL.

AUTHOR INFORMATION

Corresponding Author

Jun Wang − *Department of Pharmacology and Toxicology, College of Pharmacy, The University of Arizona, Tucson, Arizona 85721, United States; Department of Medicinal Chemistry, Ernest Mario School of Pharmacy, Rutgers, The State University of New Jersey, Piscataway, New Jersey 08854, United States;* orcid.org/0000-0002-4845-4621; Phone: 520-626-1366; Email: junwang@pharmacy.rutgers.edu; Fax: 520-626-0749

Authors

Chunlong Ma − *Department of Pharmacology and Toxicology, College of Pharmacy, The University of Arizona, Tucson, Arizona 85721, United States*

Yanmei Hu − *Department of Pharmacology and Toxicology, College of Pharmacy, The University of Arizona, Tucson, Arizona 85721, United States; Department of Medicinal Chemistry, Ernest Mario School of Pharmacy, Rutgers, The State University of New Jersey, Piscataway, New Jersey 08854, United States*

Yuyin Wang − *Department of Pharmacology and Toxicology, College of Pharmacy, The University of Arizona, Tucson, Arizona 85721, United States*

Juliana Choza − *Department of Pharmacology and Toxicology, College of Pharmacy, The University of Arizona, Tucson, Arizona 85721, United States; Department of Medicinal Chemistry, Ernest Mario School of Pharmacy,*

https://doi.org/10.1021/acsinfecdis.1c00629
ACS Infect. Dis. XXXX, XXX, XXX−XXX

Rutgers, The State University of New Jersey, Piscataway, New Jersey 08854, United States

Complete contact information is available at: https://pubs.acs.org/10.1021/acsinfecdis.1c00629

Author Contributions

[§]C.M. and Y.H. contributed equally. J.W., C.M., and Y.H. conceived and designed the study. C.M. performed the high-throughput screening, enzymatic assays, and thermal shift assay. Y.H. performed enzymatic kinetic study and FRET assays with and without BSA or preincubation. Y.W. and J.C. helped with the protein expression and purification and the enzymatic assays. J.W. wrote the manuscript with input from C.M.

Notes

The authors declare no competing financial interest.

■ ACKNOWLEDGMENTS

This research was partially supported by the National Institute of Allergy and Infectious Diseases of Health (NIH) (Grants AI147325, AI157046, and AI158775) and the Arizona Biomedical Research Commission Centre Young Investigator grant (ADHS18-198859) to J.W. The SARS-CoV-2 antiviral assay in Calu-3 cells was conducted by Drs. David Schultz and Sara Cherry at the University of Pennsylvania (USA) through the NIAID preclinical service under a nonclinical evaluation agreement.

■ REFERENCES

(1) Tregoning, J. S.; Flight, K. E.; Higham, S. L.; Wang, Z.; Pierce, B. F. Progress of the COVID-19 vaccine effort: viruses, vaccines and variants versus efficacy, effectiveness and escape. *Nat. Rev. Immunol.* **2021**, *21*, 626−636.

(2) Harvey, W. T.; Carabelli, A. M.; Jackson, B.; Gupta, R. K.; Thomson, E. C.; Harrison, E. M.; Ludden, C.; Reeve, R.; Rambaut, A.; Peacock, S. J.; Robertson, D. L. SARS-CoV-2 variants, spike mutations and immune escape. *Nat. Rev. Microbiol.* **2021**, *19*, 409−424.

(3) Beigel, J. H.; Tomashek, K. M.; Dodd, L. E.; Mehta, A. K.; Zingman, B. S.; Kalil, A. C.; Hohmann, E.; Chu, H. Y.; Luetkemeyer, A.; Kline, S.; Lopez de Castilla, D.; Finberg, R. W.; Dierberg, K.; Tapson, V.; Hsieh, L.; Patterson, T. F.; Paredes, R.; Sweeney, D. A.; Short, W. R.; Touloumi, G.; Lye, D. C.; Ohmagari, N.; Oh, Md.; Ruiz-Palacios, G. M.; Benfield, T.; Fätkenheuer, G.; Kortepeter, M. G.; Atmar, R. L.; Creech, C. B.; Lundgren, J.; Babiker, A. G.; Pett, S.; Neaton, J. D.; Burgess, T. H.; Bonnett, T.; Green, M.; Makowski, M.; Osinusi, A.; Nayak, S.; Lane, H. C. Remdesivir for the treatment of covid-19 — final report. *N. Engl. J. Med.* **2020**, *383*, 1813.

(4) Wahl, A.; Gralinski, L. E.; Johnson, C. E.; Yao, W.; Kovarova, M.; Dinnon, K. H.; Liu, H.; Madden, V. J.; Krzystek, H. M.; De, C.; White, K. K.; Gully, K.; Schäfer, A.; Zaman, T.; Leist, S. R.; Grant, P. O.; Bluemling, G. R.; Kolykhalov, A. A.; Natchus, M. G.; Askin, F. B.; Painter, G.; Browne, E. P.; Jones, C. D.; Pickles, R. J.; Baric, R. S.; Garcia, J. V. SARS-CoV-2 infection is effectively treated and prevented by EIDD-2801. *Nature* **2021**, *591*, 451−457.

(5) Cox, R. M.; Wolf, J. D.; Plemper, R. K. Therapeutically administered ribonucleoside analogue MK-4482/EIDD-2801 blocks SARS-CoV-2 transmission in ferrets. *Nat. Microbiol.* **2021**, *6*, 11−18.

(6) Sheahan, T. P.; Sims, A. C.; Zhou, S.; Graham, R. L.; Pruijssers, A. J.; Agostini, M. L.; Leist, S. R.; Schafer, A.; Dinnon, K. H., 3rd; Stevens, L. J.; Chappell, J. D.; Lu, X.; Hughes, T. M.; George, A. S.; Hill, C. S.; Montgomery, S. A.; Brown, A. J.; Bluemling, G. R.; Natchus, M. G.; Saindane, M.; Kolykhalov, A. A.; Painter, G.; Harcourt, J.; Tamin, A.; Thornburg, N. J.; Swanstrom, R.; Denison, M. R.; Baric, R. S. An orally bioavailable broad-spectrum antiviral inhibits SARS-CoV-2 in human airway epithelial cell cultures and multiple coronaviruses in mice. *Sci. Transl. Med.* **2020**, *12*, No. eabb5883.

(7) Owen, D. R.; Allerton, C. M. N.; Anderson, A. S.; Aschenbrenner, L.; Avery, M.; Berritt, S.; Boras, B.; Cardin, R. D.; Carlo, A.; Coffman, K. J.; Dantonio, A.; Di, L.; Eng, H.; Ferre, R.; Gajiwala, K. S.; Gibson, S. A.; Greasley, S. E.; Hurst, B. L.; Kadar, E. P.; Kalgutkar, A. S.; Lee, J. C.; Lee, J.; Liu, W.; Mason, S. W.; Noell, S.; Novak, J. J.; Obach, R. S.; Ogilvie, K.; Patel, N. C.; Pettersson, M.; Rai, D. K.; Reese, M. R.; Sammons, M. F.; Sathish, J. G.; Singh, R. S. P.; Steppan, C. M.; Stewart, A. E.; Tuttle, J. B.; Updyke, L.; Verhoest, P. R.; Wei, L.; Yang, Q.; Zhu, Y. An oral SARS-CoV-2 Mpro inhibitor clinical candidate for the treatment of COVID-19. *Science* **2021**, *374*, 1586−1593.

(8) Meyer, B.; Chiaravalli, J.; Gellenoncourt, S.; Brownridge, P.; Bryne, D. P.; Daly, L. A.; Grauslys, A.; Walter, M.; Agou, F.; Chakrabarti, L. A.; Craik, C. S.; Eyers, C. E.; Eyers, P. A.; Gambin, Y.; Jones, A. R.; Sierecki, E.; Verdin, E.; Vignuzzi, M.; Emmott, E. Characterising proteolysis during SARS-CoV-2 infection identifies viral cleavage sites and cellular targets with therapeutic potential. *Nat. Commun.* **2021**, *12*, No. 5553.

(9) Shin, D.; Mukherjee, R.; Grewe, D.; Bojkova, D.; Baek, K.; Bhattacharya, A.; Schulz, L.; Widera, M.; Mehdipour, A. R.; Tascher, G.; Geurink, P. P.; Wilhelm, A.; van der Heden van Noort, G. J.; Ovaa, H.; Müller, S.; Knobeloch, K. P.; Rajalingam, K.; Schulman, B. A.; Cinatl, J.; Hummer, G.; Ciesek, S.; Dikic, I. Papain-like protease regulates sars-cov-2 viral spread and innate immunity. *Nature* **2020**, *587*, 657.

(10) Báez-Santos, Y. M.; St John, S. E.; Mesecar, A. D. The SARS-coronavirus papain-like protease: structure, function and inhibition by designed antiviral compounds. *Antiviral Res.* **2015**, *115*, 21−38.

(11) Klemm, T.; Ebert, G.; Calleja, D. J.; Allison, C. C.; Richardson, L. W.; Bernardini, J. P.; Lu, B. G.; Kuchel, N. W.; Grohmann, C.; Shibata, Y.; Gan, Z. Y.; Cooney, J. P.; Doerflinger, M.; Au, A. E.; Blackmore, T. R.; van der Heden van Noort, G. J.; Geurink, P. P.; Ovaa, H.; Newman, J.; Riboldi-Tunnicliffe, A.; Czabotar, P. E.; Mitchell, J. P.; Feltham, R.; Lechtenberg, B. C.; Lowes, K. N.; Dewson, G.; Pellegrini, M.; Lessene, G.; Komander, D. Mechanism and inhibition of the papain-like protease, PLpro, of SARS-CoV-2. *EMBO J.* **2020**, *39*, No. e106275.

(12) Rut, W.; Lv, Z.; Zmudzinski, M.; Patchett, S.; Nayak, D.; Snipas, S. J.; El Oualid, F.; Huang, T. T.; Bekes, M.; Drag, M.; Olsen, S. K. Activity profiling and crystal structures of inhibitor-bound sars-cov-2 papain-like protease: A framework for anti-covid-19 drug design. *Sci. Adv.* **2020**, *6*, No. eabd4596.

(13) Shan, H.; Liu, J.; Shen, J.; Dai, J.; Xu, G.; Lu, K.; Han, C.; Wang, Y.; Xu, X.; Tong, Y.; Xiang, H.; Ai, Z.; Zhuang, G.; Hu, J.; Zhang, Z.; Li, Y.; Pan, L.; Tan, L. Development of potent and selective inhibitors targeting the papain-like protease of SARS-CoV-2. *Cell Chem. Biol.* **2021**, *28*, 855−865.e9.

(14) Shen, Z.; Ratia, K.; Cooper, L.; Kong, D.; Lee, H.; Kwon, Y.; Li, Y.; Alqarni, S.; Huang, F.; Dubrovskyi, O.; Rong, L.; Thatcher, G. R. J.; Xiong, R. Design of SARS-CoV-2 PLpro Inhibitors for COVID-19 Antiviral Therapy Leveraging Binding Cooperativity. *J. Med. Chem.* **2022**, *65*, 2940−2955.

(15) Ma, C.; Sacco, M. D.; Xia, Z.; Lambrinidis, G.; Townsend, J. A.; Hu, Y.; Meng, X.; Szeto, T.; Ba, M.; Zhang, X.; Gongora, M.; Zhang, F.; Marty, M. T.; Xiang, Y.; Kolocouris, A.; Chen, Y.; Wang, J. Discovery of SARS-CoV-2 Papain-like Protease Inhibitors through a Combination of High-Throughput Screening and a FlipGFP-Based Reporter Assay. *ACS Cent. Sci.* **2021**, *7*, 1245−1260.

(16) Ratia, K.; Kilianski, A.; Baez-Santos, Y. M.; Baker, S. C.; Mesecar, A. Structural basis for the ubiquitin-linkage specificity and deisgylating activity of sars-cov papain-like protease. *PLoS Pathog.* **2014**, *10*, No. e1004113.

(17) Fu, Z.; Huang, B.; Tang, J.; Liu, S.; Liu, M.; Ye, Y.; Liu, Z.; Xiong, Y.; Zhu, W.; Cao, D.; Li, J.; Niu, X.; Zhou, H.; Zhao, Y. J.; Zhang, G.; Huang, H. The complex structure of GRL0617 and SARS-

CoV-2 PLpro reveals a hot spot for antiviral drug discovery. *Nat. Commun.* **2021**, *12*, No. 488.
(18) Osipiuk, J.; Azizi, S. A.; Dvorkin, S.; Endres, M.; Jedrzejczak, R.; Jones, K. A.; Kang, S.; Kathayat, R. S.; Kim, Y.; Lisnyak, V. G.; Maki, S. L.; Nicolaescu, V.; Taylor, C. A.; Tesar, C.; Zhang, Y. A.; Zhou, Z.; Randall, G.; Michalska, K.; Snyder, S. A.; Dickinson, B. C.; Joachimiak, A. Structure of papain-like protease from SARS-CoV-2 and its complexes with non-covalent inhibitors. *Nat. Commun.* **2021**, *12*, No. 743.
(19) Vats, S.; Manjithaya, R. A reversible autophagy inhibitor blocks autophagosome-lysosome fusion by preventing Stx17 loading onto autophagosomes. *Mol. Biol. Cell* **2019**, *30*, 2283−2295.
(20) Ito, Y.; Fukui, M.; Kanda, M.; Morishita, K.; Shoji, Y.; Kitao, T.; Hinoi, E.; Shirahase, H. Therapeutic effects of the allosteric protein tyrosine phosphatase 1B inhibitor KY-226 on experimental diabetes and obesity via enhancements in insulin and leptin signaling in mice. *J. Pharmacol. Sci.* **2018**, *137*, 38−46.
(21) Tully, D. C.; Rucker, P. V.; Chianelli, D.; Williams, J.; Vidal, A.; Alper, P. B.; Mutnick, D.; Bursulaya, B.; Schmeits, J.; Wu, X.; Bao, D.; Zoll, J.; Kim, Y.; Groessl, T.; McNamara, P.; Seidel, H. M.; Molteni, V.; Liu, B.; Phimister, A.; Joseph, S. B.; Laffitte, B. Discovery of Tropifexor (LJN452), a Highly Potent Non-bile Acid FXR Agonist for the Treatment of Cholestatic Liver Diseases and Nonalcoholic Steatohepatitis (NASH). *J. Med. Chem.* **2017**, *60*, 9960−9973.
(22) Ma, C.; Tan, H.; Choza, J.; Wang, Y.; Wang, J. Validation and invalidation of SARS-CoV-2 main protease inhibitors using the Flip-GFP and Protease-Glo luciferase assays. *Acta Pharm. Sin. B* **2021**, DOI: 10.1016/j.apsb.2021.10.026.
(23) Ma, C.; Wang, J. Validation and invalidation of SARS-CoV-2 papain-like protease inhibitors. *ACS Pharmacol. Transl. Sci.* **2022**, *5*, 102−109.
(24) Ma, C.; Hu, Y.; Townsend, J. A.; Lagarias, P. I.; Marty, M. T.; Kolocouris, A.; Wang, J. Ebselen, Disulfiram, Carmofur, PX-12, Tideglusib, and Shikonin Are Nonspecific Promiscuous SARS-CoV-2 Main Protease Inhibitors. *ACS Pharmacol. Transl. Sci.* **2020**, *3*, 1265−1277.
(25) Ma, C.; Wang, J. Dipyridamole, chloroquine, montelukast sodium, candesartan, oxytetracycline, and atazanavir are not SARS-CoV-2 main protease inhibitors. *Proc. Natl. Acad. Sci. U.S.A.* **2021**, *118*, No. e2024420118.
(26) Xia, Z.; Sacco, M.; Hu, Y.; Ma, C.; Meng, X.; Zhang, F.; Szeto, T.; Xiang, Y.; Chen, Y.; Wang, J. Rational Design of Hybrid SARS-CoV-2 Main Protease Inhibitors Guided by the Superimposed Cocrystal Structures with the Peptidomimetic Inhibitors GC-376, Telaprevir, and Boceprevir. *ACS Pharmacol. Transl. Sci.* **2021**, *4*, 1408−1421.
(27) Li, X.; Lidsky, P. V.; Xiao, Y.; Wu, C.-T.; Garcia-Knight, M.; Yang, J.; Nakayama, T.; Nayak, J. V.; Jackson, P. K.; Andino, R.; Shu, X. Ethacridine inhibits SARS-CoV-2 by inactivating viral particles. *PLoS Pathog.* **2021**, *17*, No. e1009898.
(28) Froggatt, H. M.; Heaton, B. E.; Heaton, N. S. Development of a Fluorescence-Based, High-Throughput SARS-CoV-2 3CL(pro) Reporter Assay. *J. Virol.* **2020**, *94*, No. e01265-20.
(29) Hoffmann, M.; Kleine-Weber, H.; Schroeder, S.; Kruger, N.; Herrler, T.; Erichsen, S.; Schiergens, T. S.; Herrler, G.; Wu, N. H.; Nitsche, A.; Muller, M. A.; Drosten, C.; Pohlmann, S. SARS-CoV-2 Cell Entry Depends on ACE2 and TMPRSS2 and Is Blocked by a Clinically Proven Protease Inhibitor. *Cell* **2020**, *181*, 271−280.
(30) Kitamura, N.; Sacco, M. D.; Ma, C.; Hu, Y.; Townsend, J. A.; Meng, X.; Zhang, F.; Zhang, X.; Ba, M.; Szeto, T.; Kukuljac, A.; Marty, M. T.; Schultz, D.; Cherry, S.; Xiang, Y.; Chen, Y.; Wang, J. Expedited Approach toward the Rational Design of Noncovalent SARS-CoV-2 Main Protease Inhibitors. *J. Med. Chem.* **2022**, *65*, 2848−2865.
(31) Báez-Santos, Y. M.; Barraza, S. J.; Wilson, M. W.; Agius, M. P.; Mielech, A. M.; Davis, N. M.; Baker, S. C.; Larsen, S. D.; Mesecar, A. D. X-ray structural and biological evaluation of a series of potent and highly selective inhibitors of human coronavirus papain-like proteases. *J. Med. Chem.* **2014**, *57*, 2393−2412.
(32) Ma, C.; Sacco, M. D.; Hurst, B.; Townsend, J. A.; Hu, Y.; Szeto, T.; Zhang, X.; Tarbet, B.; Marty, M. T.; Chen, Y.; Wang, J. Boceprevir, GC-376, and calpain inhibitors II, XII inhibit SARS-CoV-2 viral replication by targeting the viral main protease. *Cell Res.* **2020**, *30*, 678−692.
(33) Cady, S. D.; Wang, J.; Wu, Y.; DeGrado, W. F.; Hong, M. Specific Binding of Adamantane Drugs and Direction of Their Polar Amines in the Pore of the Influenza M2 Transmembrane Domain in Lipid Bilayers and Dodecylphosphocholine Micelles Determined by NMR Spectroscopy. *J. Am. Chem. Soc.* **2011**, *133*, 4274−4284.
(34) Sacco, M. D.; Ma, C.; Lagarias, P.; Gao, A.; Townsend, J. A.; Meng, X.; Dube, P.; Zhang, X.; Hu, Y.; Kitamura, N.; Hurst, B.; Tarbet, B.; Marty, M. T.; Kolocouris, A.; Xiang, Y.; Chen, Y.; Wang, J. Structure and inhibition of the SARS-CoV-2 main protease reveal strategy for developing dual inhibitors against M(pro) and cathepsin L. *Sci. Adv.* **2020**, *6*, No. eabe0751.

https://doi.org/10.1021/acsinfecdis.1c00629
ACS Infect. Dis. XXXX, XXX, XXX−XXX